

**g-C₃N₄/ZnO Composite: A Emerging Photocatalyst For Dye
Degradation**

A Dissertation for
PHY-651:Dissertation

Credits: 16

Submitted in partial fulfilment of Masters degree in Physics
by

RHEA V RODRIGUES

Seat Number: 22P0430030

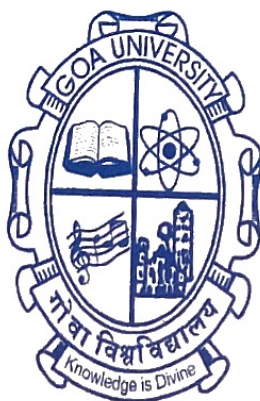
ABC ID: 829833994150

PRN: 201805031

Under the Supervision of

DR SUDHIR CHERUKULAPPURATH

School of Physical and Applied Sciences



**GOA UNIVERSITY
MAY 2024**

Examined by:

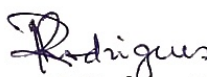


Seal of the School

DECLARATION BY STUDENT

I hereby declare that the data presented in this Dissertation report entitled, "g-C₃N₄/ZnO Composite: A Emerging Photocatalyst For Dye Degradation" is based on the results of investigations carried out by me in the Master of Physics in Science at the School of Physical and Applied Sciences at the Goa University under the Supervision of Dr Sudhir Cherukulappurath and the same has not been submitted elsewhere for the award of a degree or diploma by me. Further, I understand that Goa University or its authorities will be not be responsible for the correctness of observations / experimental or other findings given the dissertation.

I hereby authorize the University authorities to upload this dissertation on the dissertation repository or anywhere else as the UGC regulations demand and make it available to any one as needed.


Rhea V Rodrigues

22P0430030

Date: 09/05/2024


Place: Goa University

COMPLETION CERTIFICATE

This is to certify that the dissertation report "g-C₃N₄/ZnO Composite: A Emerging Photocatalyst For Dye Degradation" is a bonafide work carried out by Ms.Rhea V Rodrigues under my supervision in partial fulfilment of the requirements for the award of the degree of M.Sc in Physics at the School of Physical and Applied Sciences, Goa University.

Supervisor: Dr Sudhir Cherukulapurath

Sign: 
09th May 24



Dean: Prof. Ramesh V. Pai

School of Physical and Applied Sciences

Sign:

Date: 09/05/2024

Place: Goa University



School Stamp

Acknowledgement

I owe a debt of gratitude to Dr. Sudhir Cherukulappurath, my guide, whose knowledge, assistance, guidance and support have greatly influenced my path through this MSc Project. Not only has your mentoring improved my research, but it has also motivated me to pursue even greater academic achievements. Throughout this process, your commitment to encouraging intellectual curiosity, your forbearance during times of doubt, and your faith in my abilities have been helpful. I've been motivated to push the boundaries of my talents and aim for perfection in all I do because to your mentoring. I consider myself extremely fortunate to have had the opportunity to study under you, and I want to express my gratitude for your constant support, guidance, and devotion. Your commitment to encouraging inquisitiveness and your patience. My sincere gratitude goes out to my Ph.D. guide, Ms . Namita , whose commitment, teamwork, and priceless contributions have been essential to the accomplishment of our research projects. Our academic path has been both enjoyable and rewarding because of your love for learning and dedication to greatness.

I appreciate your friendship, support, and joint quest of knowledge. This accomplishment is evidence of our group's hard work and spirit of cooperation. Even at my darkest hours, and your faith in my abilities has been so helpful to me all along this journey. I've been motivated to push the boundaries of my talents and aim for perfection in all I do because to your mentoring. I would also take this opportunity to thank all the other ph.D students you have helped me in numerous ways to make this project a successful one.

Abstract

Photocatalysis has become a promising technology in the search for environmentally remedial and sustainable energy sources. Because of its special qualities and possible uses, the composite of zinc oxide (ZnO) and graphitic carbon nitride (g-C₃N₄) has attracted a lot of interest among photocatalysts. A thorough analysis of the state of the art research on g-C₃N₄ in bulk and g-C₃N₄/ZnO as a developing photocatalyst is presented in this abstract. The abstract explores the basic ideas of photocatalysis and clarifies the processes that lead to the production and application of photoexcited charge carriers. Optimizing the performance and design of photocatalysts requires a thorough understanding of these mechanisms. The synthesis procedures for creating g-C₃N₄ in bulk and g-C₃N₄/ZnO composites are then covered. Additionally emphasized is the impact of synthesis factors on the physiochemical characteristics of bulk g-C₃N₄ and g-C₃N₄/ZnO composites. Characterization methods such as photoluminescence (PL), UV-Vis absorbance spectroscopy, and Powder X-ray diffraction (PXRD) are used. In the following section, the optical characteristics of bulk g-C₃N₄ and g-C₃N₄ composites are discussed. These composites' optical absorption characteristics and bandgap engineering are key factors in defining their photocatalytic performance. Utilizing methods including photoluminescence and UV-visible DRS spectroscopy, researchers examine the optical characteristics of g-C₃N₄ in bulk and g-C₃N₄ composites. The difficulties and potential outcomes in the creation of bulk g-C₃N₄ and g-C₃N₄/ZnO composites as photocatalysts are finally described. Overcoming the various obstacles will enable the broad use of g-C₃N₄ in bulk and g-C₃N₄/ZnO composites in photocatalysis. The article concludes by offering a thorough summary of the most recent developments in the synthesis, characterisation, and photocatalytic uses of g-C₃N₄ and g-C₃N₄/ZnO composites in bulk.

List of Tables

2.1	Synthesis trial for g-C ₃ N ₄	13
2.2	Displays the various trials for synthesising bulk g-C ₃ N ₄ /ZnO composite. .	17
4.1	Displays the absorbance peak and the band gap for ZnO, g-C ₃ N ₄ and the composite	31
4.2	The various photocatalytic studies that are done by varying various parameters.	38
4.3	The Rate Constant and the % Degrdation to the corresponding Sample.	39

List of Figures

2.1	Methylene Blue dye	7
2.2	the Tube Furnace that was used and the g-C ₃ N ₄ solid sample that was obtained.	8
2.3	Solid g-C ₃ N ₄ sample obtained using Melamine as the precursor	9
2.4	Displays solid g-C ₃ N ₄ samples synthesized at 450°C, 550°C and 650°C. . . .	10
2.5	Oven used for calcinating the samples.	11
2.6	XRD of g-C ₃ N ₄ /ZnO Composite Trial 1	13
2.7	XRD of g-C ₃ N ₄ /ZnO Composite Trial 2	14
2.8	XRD of g-C ₃ N ₄ /ZnO Composite Trial 5	16
2.9	Obtained Solid Samples for g-C ₃ N ₄ /ZnO	17
2.10	Photocatalytic Dark studies.	18
2.11	Photoreactor Setup.	19
3.1	PXRD Setup	21
3.2	Schematics of Raman Setup	22
3.3	UV DRS Setup	25
3.4	Photoluminescence Setup	25
3.5	Flourescence Setup	26
4.1	XRD graph for Bulk g-C ₃ N ₄ /ZnO, bulk g-C ₃ N ₄ and bulk ZnO	28
4.2	Raman Graph for g-C ₃ N ₄	29
4.3	UV - DRS graph for Bulk g-C ₃ N ₄ , bulk ZnO and bulk g-C ₃ N ₄ /ZnO	30

4.4	Tauc's plot for direct band gap for Bulk g-C ₃ N ₄ , bulk ZnO and g-C ₃ N ₄ /ZnO composite respectively	31
4.5	PL graph for(a) Bulk g-C ₃ N ₄ (b) calc. g-C ₃ N ₄ and (c) comparision of g-C ₃ N ₄ and g-C ₃ N ₄ /ZnO	32
4.6	PL graph for(a) Bulk g-C ₃ N ₄ (left) and Calc. g-C ₃ N ₄ (right) b) Bulk ZnO and (c) bullk g-C ₃ N ₄ /ZnO and Calc.bulk g-C ₃ N ₄ /ZnO	34
4.7	Photo degradation Graph for(a) MB Dye ,(b) Calc. ZnO , (c) Bulk g-C ₃ N ₄ ,(d)calc. g-C ₃ N ₄ , (e) Bulk g-C ₃ N ₄ /ZnO , (f) Calc. g-C ₃ N ₄ /ZnO . . .	37
4.8	Graph of A/Ao versus time (mins)	38
4.9	Colour degradation Graph for(a) MB Dye ,(b) Calc. ZnO , (c) Bulk g-C ₃ N ₄ ,(d) calc. g-C ₃ N ₄ , (e) Bulk g-C ₃ N ₄ /ZnO , (f) Calc. g-C ₃ N ₄ /ZnO . .	39

Contents

List of Tables	iii
List of Figures	iv
1 Introduction	1
1.1 2D Materials	3
1.2 Graphitic Carbon Nitride	3
1.3 ZnO	4
1.4 g-C ₃ N ₄ /ZnO Composite	5
1.5 Objectives	6
2 Experimental	7
2.0.1 Chemicals	7
2.0.2 Synthesis of g-C ₃ N ₄ using thiourea as the starting precursor	8
2.0.3 Synthesis of g-C ₃ N ₄ using melamine as the starting precursor	9
2.0.4 Synthesising g-C ₃ N ₄ at various temperature using melamine as the precursor.	10
2.0.5 Calcination	11
2.0.6 Synthesis of g-C ₃ N ₄ /ZnO	13
2.0.7 Photocatalytic Activity	17
3 Instrumentation	20
3.0.1 Powder X- Ray Diffraction (PXRD)	20

3.0.2	Raman Spectroscopy	22
3.0.3	UV Diffuse Reflectance spectroscopy(UV DRS)	24
3.0.4	Photoluminescence (PL)	24
3.0.5	Flourescence	26
4	Results and Discussion	27
4.0.1	Characterisations	27
4.0.2	PXRD Analysis	27
4.0.3	Raman Spectroscopy	28
4.0.4	Optical Properties	29
4.0.5	PL Study	32
4.0.6	Flourescence	34
4.0.7	Photocatalytic Performance	35
4.1	Factors affecting photocatalytic Activity	40
4.1.1	Effect of initial dye concentration	40
4.1.2	Effect of catalyst Dose Amount	40
4.1.3	Effect of Calcination on bulk sample	41
4.2	Mechanism	42
4.2.1	Mechanism of a photocatalyst	42
4.2.2	Mechanism of g-C ₃ N ₄ as a photocatalyst	42
4.2.3	Mechanism of g-C ₃ N ₄ /ZnO as a photocatalyst	43
	References	44

Chapter 1

Introduction

The world is under stress due to the declining quality of water with each day that goes by, which is caused by the increase in human population, industrialization, and other activities. Since wastewater treatment is a serious issue, developing strategies for it should be of the utmost importance. With growing industrialization and urbanization, there is growing worry over synthetic dye releases into the environment due to their detrimental effects on ecosystems and human health. Synthetic dyes are widely used in many different industries, including paper, plastics, textiles, and cosmetics, to give goods color. However, the reckless discharge of wastewater containing dyes into aquatic environments poses a major threat to aquatic ecosystems and human health. Due to their resistance to biodegradation, many synthetic dyes can persist in the environment for extended periods of time, contaminating water, disrupting ecosystems, and harming human health. Traditional color degradation methods can turn out to be inefficient or harmful to the environment.

In this context, the use of photocatalysts for dye degradation has emerged as a workable solution that offers a sustainable way to lessen the consequences of dye pollution. This introduction seeks to highlight the critical role that photocatalysts play in the degradation of synthetic dyes, with an emphasis on current advancements and their fundamental significance in tackling today's environmental challenges. The method of photocatalysis,

which breaks down organic pollutants like artificial colors by using light energy to accelerate chemical reactions, offers a practical and effective way to do so [1]

Photocatalysts are usually semiconducting materials such as titanium dioxide (TiO_2), zinc oxide (ZnO), and graphitic carbon nitride ($\text{g-C}_3\text{N}_4$). These materials can produce reactive oxygen species (ROS) when exposed to the right kind of light. ROS can then oxidize and mineralize organic pollutants, including synthetic dyes, into harmless byproducts like carbon dioxide and water. Recent research efforts have focused on improving the photocatalytic efficiency and selectivity for dye degradation of semiconductor photocatalysts. Advanced synthesis techniques such as sol-gel, hydrothermal, and microwave-assisted synthesis have been employed to change the surface properties, crystallinity, and morphology of photocatalysts to improve their catalytic efficiency. Moreover, their effectiveness in degrading a range of synthetic dyes in various environmental conditions has grown with the development of novel heterostructures, doping strategies, and photocatalyst composites [2].

Using photocatalysts to degrade dyes is an environmentally friendly method of reducing dye pollution, but it has a significant environmental impact. Photocatalysis uses solar energy as the catalyst for dye degradation, reducing the amount of harmful byproducts produced and reducing reliance on external energy sources. Photocatalytic dye degradation has come a long way, yet there are still many problems that need to be overcome [1]. These include improving photocatalytic reactor designs and operating conditions for practical applications and developing more stable, efficient, and recyclable photocatalysts. Future studies on photocatalysis for dye degradation should focus on finding solutions to these issues while exploring novel photocatalytic materials, procedures, and reactor configurations. Two-dimensional materials have shown to be the most appropriate of all the material types for photocatalysis.

1.1 2D Materials

One-layer, or two-dimensional, crystalline solids consisting of a single layer of atoms are called single-layer materials. Two-dimensional materials are a part of a larger class of nanomaterials that are identified by their dimensions, or more accurately, by being in the nanoscale range. These materials differ from their 3D counterparts in that they have a thin atomic structure, sometimes comprising only a few or even a single atom. The extremely thin structure of 2D materials gives rise to their unique features [3]. These 2D materials have exceptional physical and chemical properties, which are different from bulk 3D materials, with a high surface area-to-volume ratio, remarkable mechanical strength, and superior electronic conductivity.

These have sparked a great deal of curiosity among scientists and resulted in creative applications across a range of disciplines. The enormous surface area of 2D materials is one of their key features; this makes them perfect for catalytic processes [4]. Its superior electrical conductivity also makes it easier to utilize in electronics and energy-storage systems. Since 2D materials are thin, flat structures, new materials with unique properties can be created by stacking or layering them in various configurations to form what are known as van der Waals heterostructures. This creates fresh opportunities for creative applications

1.2 Graphitic Carbon Nitride

$g - C_3N_4$ has emerged as a potential semiconductor material with a broad variety of applications in photocatalysis due to its unique properties and intrinsic stability. In recent times, there has been a notable progress in comprehending the fundamental concepts, manufacturing techniques, and practical applications of $g-C_3N_4$ as a photocatalyst. This introduction aims to provide an overview of recent advancements in $g-C_3N_4$ photocatalytic application advances, highlighting the material's potential to address pressing environmental and energy-related issues. Due to its unique electrical structure and suitable bandgap for light absorption, $g-C_3N_4$ is capable of photocatalysis using solar en-

ergy. Visible light response element g-C₃N₄ has a band gap of 2.7 eV, while CB and VB's energy locations are at 1.1 and 1.6 eV.

Recent studies have provided insights into the band structure and electrical properties of g-C₃N₄, providing information on its photocatalytic activity. Unlike other metal-containing photocatalysts, g-C₃N₄ has the unique capacity to be easily synthesized by thermally polycondensing the inexpensive N-rich precursors, such as dicyanamide, cyanamide, melamine, melamine, and urea. One of the main advantages of g-C₃N₄ is its exceptional chemical stability, which allows it to withstand harsh reaction conditions and prolonged exposure to light without significantly degrading. This property makes g-C₃N₄ a desirable choice for long-term photocatalytic applications. To boost g-C₃N₄'s selectivity and photocatalytic activity for specific processes, its surface chemistry and shape can be changed.

Advances in surface modification techniques have allowed for the controlled synthesis of g-C₃N₄ with ideal surface properties for photocatalysis. The initial method used to produce g-C₃N₄ was thermal condensation of precursor compounds such as urea or melamine. These methods, while effective, often resulted in g-C₃N₄ with low crystallinity and surface area. Advancements in synthesis techniques, including template-assisted, hydrothermal, and solvothermal procedures, have enabled the production of g-C₃N₄ with improved shape, surface features, and crystallinity.

1.3 ZnO

Zinc oxide (ZnO) has become a widely used semiconductor material in a variety of industries, including photocatalysis. Zinc oxide (ZnO) is an important flexible photocatalyst, and its significance has been highlighted by recent advances in understanding its fundamental characteristics, production methods, and photocatalytic mechanisms. The purpose of this introduction is to give a summary of current research on the application of ZnO as a photocatalyst and to emphasize the potential of this material in resolving current environmental and energy-related issues. 3.37 eV is a big band gap for zinc oxide. Zinc oxide (ZnO) is an excellent UV optical transparent material with a broad bandgap that makes it suitable for photocatalytic activities[5].

Recent studies have shed light on ZnO's band structure and optical properties, revealing information about how well the material functions as a photocatalyst under different lighting conditions. The ZnO surface has a variety of surface states, reactive sites, and defects, all of which are necessary for encouraging photocatalytic reactions. Improvements in defect management and surface engineering have led to an increase in ZnO's catalytic activity and surface reactivity, improving photocatalytic performance. Zinc Oxide (ZnO) is suitable for long-term photocatalytic applications due to its remarkable chemical stability and durability in a variety of environmental conditions. Recent studies have looked at the stability mechanisms of zinc oxide (ZnO) and strategies to increase its resistance to photocorrosion and degradation during photocatalysis[6].

1.4 g-C₃N₄/ZnO Composite

When g-C₃N₄ and ZnO are combined in nanocomposite structures, their synergistic effects enhance their photocatalytic activity. The tight contact between g-C₃N₄ and ZnO facilitates efficient charge separation and transfer under both UV and visible light irradiation, enhancing photocatalytic activity. Recent studies have demonstrated that g-C₃N₄/ZnO nanocomposites perform better than their individual components for a range of photocatalytic applications.

A potential family of photocatalytic materials with a variety of uses in solar energy conversion and environmental remediation are g-C₃N₄/ZnO nanocomposites. Recent advancements in the synthesis, characterization, and photocatalytic performance of g-C₃N₄/ZnO nanocomposites have opened up new avenues for addressing global challenges related to water pollution. The goal of study is to create effective and long-lasting photocatalytic systems for a cleaner and more sustainable future by utilizing the complementary properties of g-C₃N₄ and ZnO.

1.5 Objectives

The aim of this study is to examine the possible uses and effectiveness of photocatalysts in the breakdown of synthetic dyes. Methylene blue dye is the dye that was employed in this research work to examine the degradation. The study's specific objectives are to :

- synthesize g-C₃N₄ and the g-C₃N₄/ZnO composite
- Characterizations
- examine its photocatalytic activity
- To study Factors affecting the photocatalytic performance
- its mechanism and function in pollutant degradation

The study aims to clarify the parameters affecting photocatalytic activity, such as the quantity of catalyst being utilized and the properties of the light source, by experimental evaluation and theoretical modeling.

Chapter 2

Experimental

2.0.1 Chemicals

All the chemicals used for the synthesis of pure $g\text{-C}_3\text{N}_4$, $g\text{-C}_3\text{N}_4/\text{ZnO}$ such as melamine ($\text{C}-3\text{H}_6\text{N}_6$), zinc acetate dehydrate ($(\text{CH}_3\text{COO})_2\text{Zn} \cdot 2\text{H}_2\text{O}$) were the starting precursors and were purchased from Sigma Aldrich and s d fine-chem limited (SDFCL) respectively, ethanol ($\text{C}_2\text{H}_5\text{OH}$) and distilled water was used for washing purpose. Methylene Blue Dye was purchased from Avantor Performance Materials India Limited. Throughout the experiment, distilled water was used.



Figure 2.1: Methylene Blue dye

2.0.2 Synthesis of g- C_3N_4 using thiourea as the starting precursor

To synthesize g- C_3N_4 , thiourea was utilized as the initial ingredient. In this case, thiourea serves as a precursor. The weighing equipment was used to weigh 10 gms of thiourea. This was then moved to a ceramic crucible. The ceramic lid sealed the crucible completely. This was then placed in a tube furnace with a ceramic crucible on top of a rectangular plate. The following were the tube furnace operating conditions: heated at 550 °C at a rate of 2 °C/min for 4 hrs. A mortar and pestle was used to form a powder form of the yellow solid sample that was obtained. The above yellow coloured powder was used for further characterization. A similar procedure was tried using Melamine as the precursor [7].

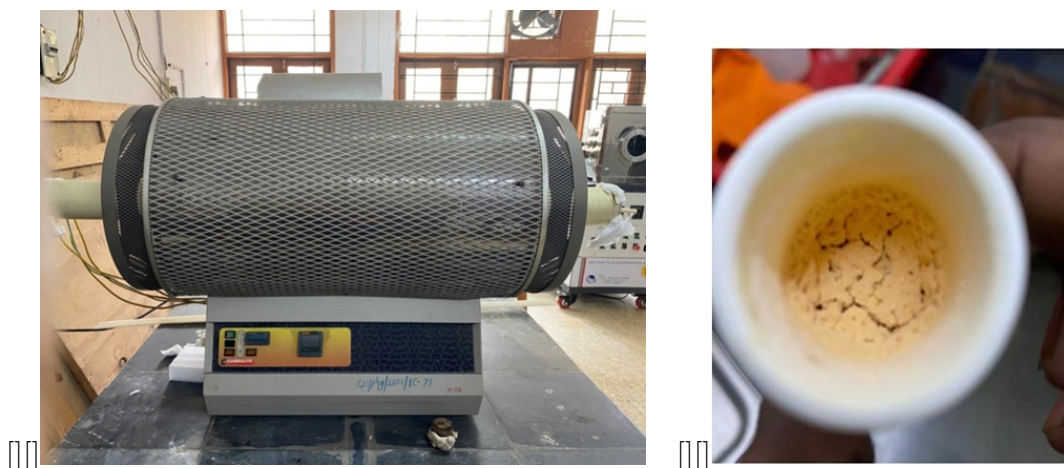


Figure 2.2: the Tube Furnace that was used and the g- C_3N_4 solid sample that was obtained.

2.0.3 Synthesis of g-C₃N₄ using melamine as the starting precursor

Take 10 g of melamine put in the ceramic crucible and cover it with a lid. Put the crucible in tube furnace. In this case, the tube furnace wherein the rate had to be manually set was used. Set the parameters as temperature 550 °C for 4hr with heating rate of 2 °C /min. Once the temperature was reached to 550°C, the furnace was switched off and the sample was left overnight so that it was allowed to come back to room temperature naturally. Once the furnace came back to room temperature, the sample was removed from the furnace. Solid sample was obtained which was further grinded in order to obtain the powder[7].



Figure 2.3: Solid g-C₃N₄ sample obtained using Melamine as the precursor

2.0.4 Synthesising $g\text{-C}_3\text{N}_4$ at various temperature using melamine as the precursor.

Trial 1

Take 10 g of melamine put in the ceramic crucible and cover it with a lid. Put the crucible in tube furnace. In this case, the tube furnace wherein the rate had to be manually set was used. Set the parameters as temperature 450°C for 4hr with heating rate of $2^\circ\text{C}/\text{min}$. Once the temperature was reached to 450°C , the furnace was switched off and the sample was left overnight so that it was allowed to come back to room temperature naturally. Once the furnace came back to room temperature, the sample was removed from the furnace. Solid sample was obtained which was further grinded in order to obtain the powder. The above same procedure was used for synthesizing at 650°C as well. [8].

At 450°C , White colour sample was obtained.

At 650°C , dark yellow colour sample was obtained.

Result: In the above case, the sample was not completely formed as the intermediate products of melamine were also seen in the XRD. The rate plays a very crucial role in synthesizing and one of the reasons why the sample was not completely formed could be because the rate was not constant throughout.



Figure 2.4: Displays solid $g\text{-C}_3\text{N}_4$ samples synthesized at 450°C , 550°C and 650°C .

2.0.5 Calcination

To obtain Bulk g-C₃N₄ and Calcinated g-C₃N₄/ZnO Samples



Figure 2.5: Oven used for calcinating the samples.

Take the solid sample and grind out a little with the help of a mortar and pestle. Take approximately 500 mg of the prepared g-C₃N₄ and put in ceramic crucible and cover the crucible with ceramic lid [6]. Place this crucible in Oven and set the parameters as heating temperature 250 °C with heating rate 2 °C/min for 2 hrs. Wait till the temperature of oven reaches to 250 °C once it reaches put off the oven and the sample was allowed to come down to room temperature naturally overnight. This sample was further used for the photocatalytic study. This exact same procedure was used for calcinating g-C₃N₄/ZnO as well. [7].

Why Melamine is a better precursor compared to thiourea?

Melamine is often considered a better precursor than thiourea for the synthesis of graphitic carbon nitride due to several factors:

- Nitrogen Content:

Nitrogen is the most essential component of g-C₃N₄ lattice. the presence of these nitrogen atom in the lattice structure act as the active sites for catalytic reactions.

- Structural Stability:

The carbon nitrogen bonds that are present in the triazine rings are way more stronger ,thus providing more stability to the molecule. The presence of these nitrogen atom in the triazine ring eventually increases the number of covalent bond present. In thiourea, the Carbon sulphur bonds are comparatively weaker than carbon nitrogen bond.

- Photocatalytic Performance:

More nitrogen content provides more active sites for photocatalytic reactions.

- Yield:

The final yield obtained using Melamine as the precursor is way more than that obtained using thiourea as the precursor.

Why 550°C was considered to be the optimizing temperature for the synthesis?

As per [9], The increase in the heating temperature can enlarge the bandgap of g-C₃N₄. When the calcinating temperature was increased from 2.77 eV - 2.77 eV because of increased degree of polymerisation. When the temperature was further increased to 650°C ,the band gap further increased to 2.82 eV [6]. This revealed that the band gap in case of g-C₃N₄ at 550°C was narrower than samples prepared in the range 450°C -650°C. Also, the sample synthesized at 550°C had higher ability of absorbing visible light which can further lead to better photocatalytic activity[5].

TRIAL	PRECURSOR	QT. gm	CRUCIBLE LID	TEMPERATURE °C	HEATING RATE	RESULT
1	Thiourea	1	Semi closed	550	2	Evaporated
2	Thiourea	2	Semi closed	550	15	Evaporated
3	Thiourea	10	closed	550	2 (Constant)	Sample is formed
4	calc. g-C ₃ N ₄ (thiourea) @ 250 2					
5	Melamine	10	closed	550	2	Sample is Not Formed
6	melamine	3	closed	650	5	Sample is not formed
7	Melamine	3	closed	450	5	Not formed
8	Calc. g-C ₃ N ₄ (Melamine) @250 2					
9	Melamine	10	closed	550	2 (Constant)	Sample is formed

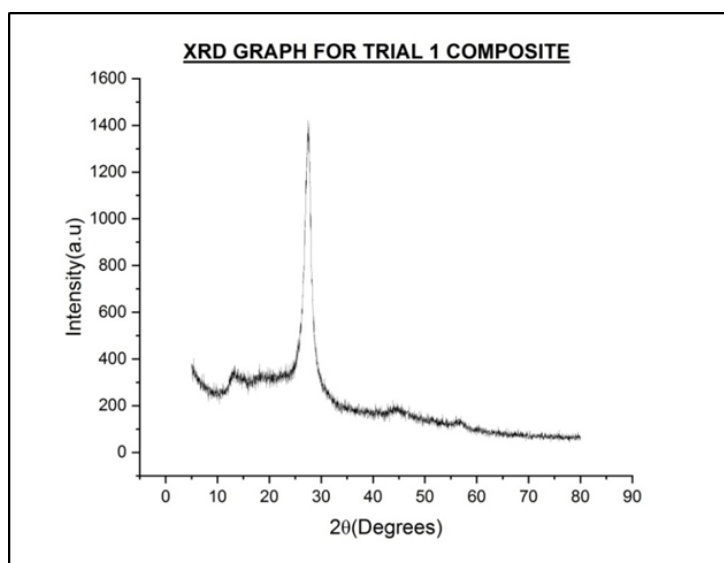
Table 2.1: Synthesis trial for g-C₃N₄

2.0.6 Synthesis of g-C₃N₄/ZnO

Trial 1

Weighed 5 gms of Melamine and 1.25 gms of zinc acetate dehydrate .Grind them well for 30-45 mins. Place it in the oven for 1 hr at 85 °C. Place it in the furnace at 550 °C for 3 hrs at 2 °C/min with a partially closed lid and was then allowed to come back to room temperature. The obtained yellow coloured powder was then crushed and grinded. Wash the obtained powder with 0.1 M of HNO₃, distilled water and ethanol. The powder was then placed in an oven at 85 °C for 5 hrs[10].

Result : This above procedure did not work for the synthesis of the composite. Only g-C₃N₄ peak were seen in the XRD and no ZnO peaks were visible indicating the absence of ZnO in the composite.

Figure 2.6: XRD of g-C₃N₄/ZnO Composite Trial 1

Trial 2

Precursors, zinc acetate and melamine, were utilized to create g-C₃N₄ /ZnO composite photo catalysts. In a standard run, 10g of melamine powder was added after 20 ml of deionized water had been used to dissolve zinc acetate (0.125 g, 0.57 mmol). Melamine was dissolved in zinc acetate solution and agitated vigorously for one hour. The mixture was then vacuum-dried for four hours at 80 °C. The resulting mashed mixture was then placed in a covered crucible and heated for two hours at 500 °C at a heating rate of 20 °C min⁻¹ in a muffle furnace [11].

Result :This above procedure did not work for the synthesis of the composite.

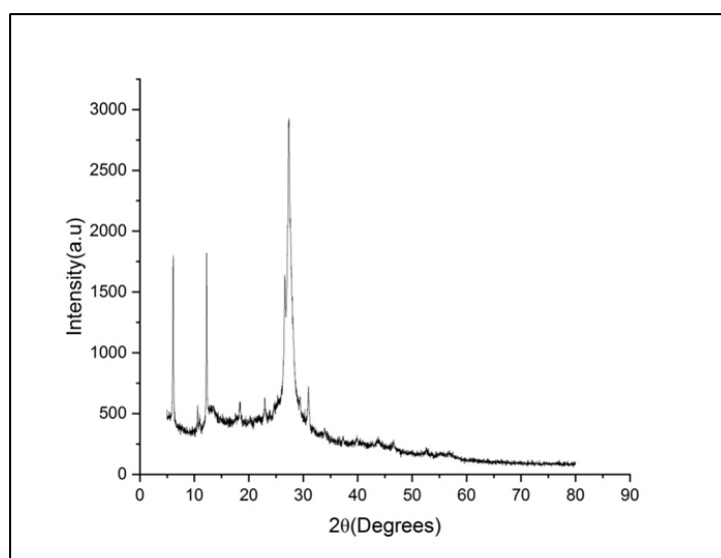


Figure 2.7: XRD of g-C₃N₄/ZnO Composite Trial 2

Trial 3

6 gms of Melamine and 3 gms of zinc acetate dehydrate .This mixture was grinded with the help of a mortar pestle for about an hour.This mixture was then shifted to a ceramic crucible and placed in a furnace 550 °C for 4 hrs.The final product was then washed with ethanol and dried at 80 °C for 3 hrs in a oven [10].

Result : This above procedure did not work for the synthesis of the composite. Only g-C₃N₄ peak were seen in the Xrd and no ZnO peaks were visible indicating the absence of ZnO in the composite.

Trial 4

Weighed 10 gms of melamine and 0.125 gms of zinc acetate dehydrate. Measure 20 ml of distilled water and pour the measured zinc acetate into it and dissolve it in water completely. Stir it for an hour or so Dry it in the oven at 80 °C for 4 hr. After drying, grind the white powder, transfer it in a crucible and place it in the furnace with a completely closed lid at 500 °C for 2 hr at 2 °C /min.The obtained sample was then grinded into powder [11].

Result : This above procedure did not work for the synthesis of the composite.

Trial 5

Weigh 9 gms of melamine and 1.8 gms of Zinc Oxide (20 percent of Zinc Oxide). Grind it for some time using mortar and pestle. Transfer the grinded mixture into a ceramic crucible with a completely closed lid. Place it in the furnace at 550°C for 4 hrs at 5°C/min [12].

Result : This above procedure did work for the synthesis of the composite but the intensities of the peak were too high.

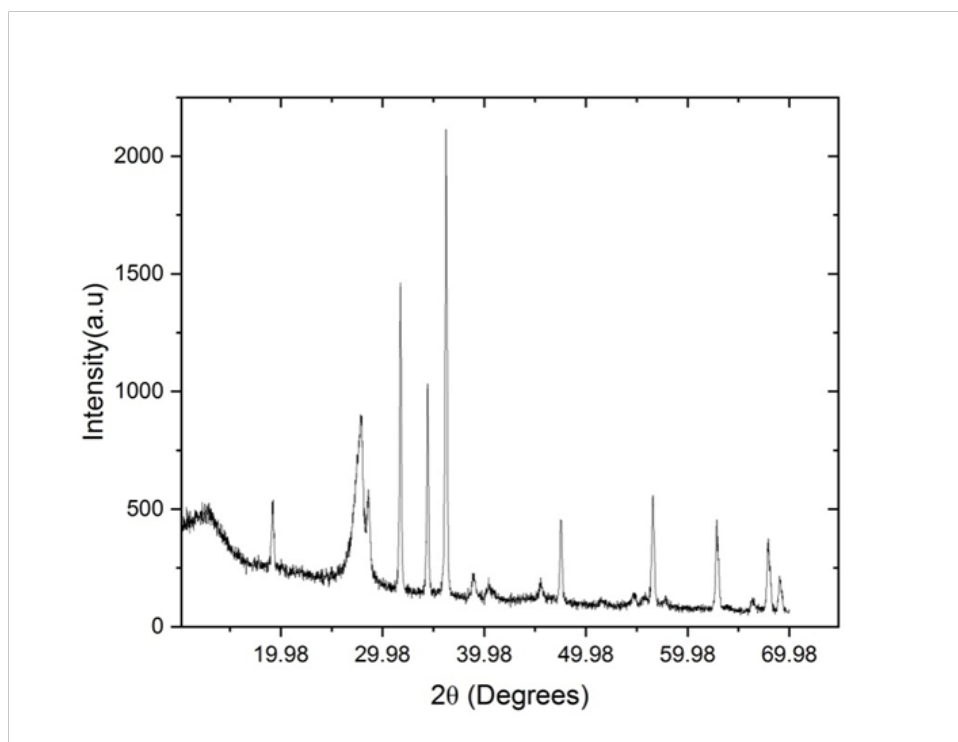


Figure 2.8: XRD of g-C₃N₄/ZnO Composite Trial 5

Trial 6

Weigh 7 gms of melamine and 3.5 gms of Zinc Oxide (50 of Zinc Oxide). Grind it for some time using mortar and pestle. Transfer the grinded mixture into a ceramic crucible with a completely closed lid. Place it in the furnace at 550°C for 4 hrs at 2°C /min [12].

Result :The g-C₃N₄/ZnO composite was successfully obtained using the above trial 6 procedure.



Figure 2.9: Obtained Solid Samples for g-C₃N₄/ZnO

TRIAL	PRECURSOR	QT. (gm)	CRUCIBLE LID	TEMP. °C	HEAT. RATE	RESULT
1	Melamine/ Zinc Acetate	5/ 1.25	Semi Closed	550	2	Not formed
2	Melamine/ Zinc Acetate	10/ 0.125	Semi closed	500	20	Not formed
3	Melamine/ Zinc Acetate	6/3	Closed	550	5	Sample not formed
4	Melamine/ Zinc Acetate	10/ 0.125	Closed	500	2	Not formed
5	Melamine/ Zinc Oxide	9/ 1.8	Closed	550	2	formed
6	Melamine/ Zinc Oxide	7/ 3.5	Closed	550	2	formed

Table 2.2: Displays the various trials for synthesising bulk g-C₃N₄/ZnO composite.

2.0.7 Photocatalytic Activity

Here, the 10 ppm of MB dye solution was prepared as below. Firstly, a 1000 ppm stock solution was prepared where in 0.1 gm of g-C₃N₄ was dissolved in 100 ml of water. Then from this 1000 ppm of stock solution was prepared. Now, for 10 ppm, 1 ml from 1000 ppm stock solution was again dissolved in 100 ml of water.

FORMULA TO PREPARE STOCK SOLUTION

$$ppm = (gmsofsolute/ml of solution) * 100$$

The Methylene Blue Dye breakdown test was used to assess the photocatalytic activity of the as-prepared samples under visible light irradiation. A visible bulb supplied the visible light. A glass vessel in a photoreactor setup was filled with an aqueous solution of MB (10 ppm), and 100 mg of photocatalyst was added. To achieve the saturation absorption of MB onto the catalysts, the suspensions were magnetically agitated in the dark for approximately 45 minutes after being subjected to ultrasonication for about 15 minutes prior to irradiation. The photoreactor with the visible lamp was then filled with this solution. After the adsorption was finished, turn on the lamp. Three milliliters of sample solution were sampled at specific intervals. Using a UV–Vis spectrophotometer, the filtrates were examined for differences in the highest absorption peak (650 nm for MB). Also, various studies keeping the ppm fixed and by varying the amount of g-C₃N₄ was also studied using a Visible lamp in order to optimise the amount of g-C₃N₄ and the composite.



Figure 2.10: Photocatalytic Dark studies.



Figure 2.11: Photoreactor Setup.

Chapter 3

Instrumentation

3.0.1 Powder X- Ray Diffraction (PXRD)

An X-ray source, a sample holder, an XRD detector are the three primary components of an X-ray apparatus. The source illuminates the sample with X-rays. After that, it passes through the sample phase and into the detector. The intensity is measured and diffraction data are recorded by moving the tube or sample and detector to alter the diffraction angle (2θ), which is the angle between the incident and diffracted beams. The angle between the incident beam and the sample can be either constant or variable, depending on the diffractometer's geometry and the kind of sample. This angle is typically associated with the diffracted beam angle.

Using this method, x-ray beams are passed through it[4]. Instead of utilizing considerably longer wavelengths, which would remain unchanged by the spacing between atoms, X-ray beams are chosen because their wavelength is similar to the spacing between atoms in the sample. As a result, the angle of diffraction will be modified by the spacing of the atoms in the molecule. Following their passage through the sample, the x-rays "bouncing" off of the atoms in the structure cause the beam to change direction at an angle, θ , that differs from the initial beam. This is the diffraction angle.

While some of these diffracted beams cancel each other out, positive interference happens when the beams have wavelengths in common. When two x-ray beams with whole number integer wavelengths combine to form a new beam with a larger amplitude, this is known as constructive interference. For this particular angle of diffraction, a larger signal corresponds with a larger wave amplitude. The difference between atomic planes can then be calculated using the angle of diffraction and Bragg's rule,

$$[2d\sin\theta = n\lambda$$

where d is the distance between atomic planes, λ is the wavelength added, and θ is the angle of diffraction. The composition or crystalline structure can then be ascertained by measuring the distance between atomic plates.[13]

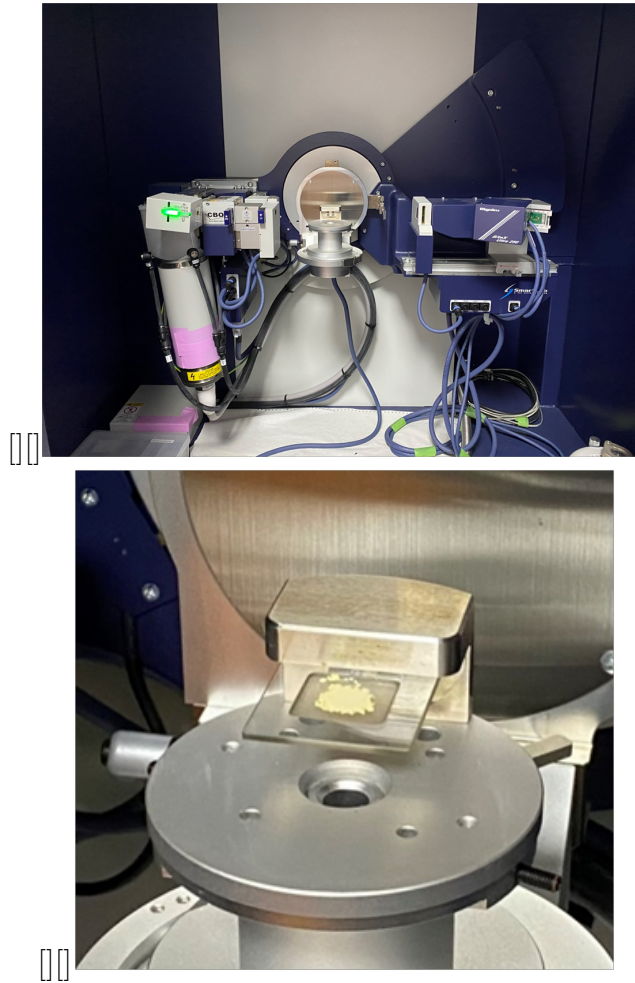


Figure 3.1: PXRD Setup

3.0.2 Raman Spectroscopy

An essential method for classifying various materials—which can be solids, liquids, or gases—is Raman spectroscopy. It is a straightforward, non-invasive method that doesn't need complex sample preparation. A spectrometer analyzes the dispersed light after the sample is exposed to monochromatic light. This method uses the monochromatic light's inelastic scattering. The incident photons' frequency varies during the scattering process. The sample absorbs input light photons before reemitting them. These photons' frequency shifts in relation to the fundamental monochromatic frequency, either upwards or downwards. We refer to this phenomena as the Raman effect. Important details on the vibrational, rotational, and low frequency transitions of the sample molecules are contained in these shifts.

The characteristic frequency ν_o is the vibration frequency of molecules caused by periodic deformation. Therefore, the molecules are excited by the monochromatic laser beam with frequency ν_o , which transforms them into oscillating dipoles.

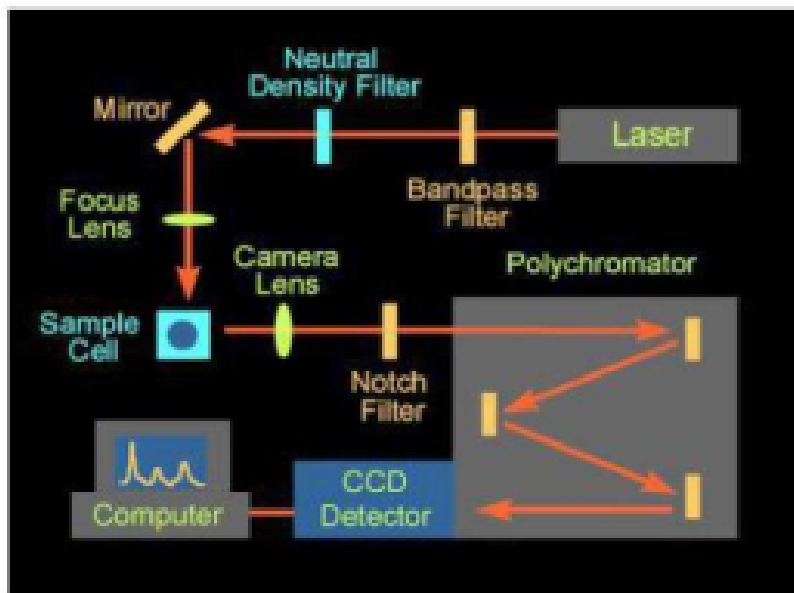


Figure 3.2: Schematics of Raman Setup

From fig 13, The essential parts of a Raman spectrophotometer are:

- Laser:

Mercury arc lamps were utilized as the light source in early Raman spectrometers; until the 1960s, a 435.8 nm line of coiled low-pressure mercury arc lamp was in use. When laser sources became widely available in the late 1960s, mercury lamps were totally replaced. These laser sources emit a steady, powerful beam of light. Many different types of lasers are available for use, such as Neodymium-Yttrium Aluminum Garnet (Nd:YAG) and Neodymium-Yttrium Ortho-Vanadate (Nd:YVO₄) (1064 nm), Argon ion (488 and 514.5 nm), Krypton ion (530.9 and 647.1 nm), Helium-Neon (He-Ne) (632.8 nm), Near Infrared (IR) diode lasers (785 and 830 nm), as well as other types of lasers. Short wavelength sources, such as argon and krypton ion lasers, produce a significant amount of fluorescence and cause the specimen to photodegrade.

- Optics for sample illumination and light collection:

To obtain the Raman spectrum, light from the irradiated or lit spot is collimated by a lens and directed into an interference filter or spectrometer.

- Spectrometer or filter used as a wavelength selector:

One laser beam can be separated using band pass filters. Dispersive instruments often use a grating monochromator of superior quality in conjunction with a notch filter. To distinguish between strong Rayleigh scattered radiations and comparatively weak Raman lines, devices such as double or even triple grating monochromators, super notch filters, rejection filters, holographic notch or edge filters, and holographic filters are employed.

- Detector:

Early dispersive Raman spectrophotometer models featured photodiode array detectors and thermoelectrically cooled photomultiplier tubes. These detectors are replaced by more sensitive charge transfer devices (CTDs), such as charge-coupled

devices (CCDs) and charge-injection devices (CIDs), thanks to developments in instrumentation and technology. These devices are employed in array form and function as detectors. The photosite in CTD arrays transforms the incoming optical signal into charge, which is then integrated and sent to the readout devices. When the laser wavelength is less than 1 μm , multichannel CCD detectors are utilized, and when the laser wavelength is larger than 1 μm , single element narrow band-gap semiconductor detectors like Germanium (Ge) or Indium–Gallium–Arsenic (InGaAs) detectors are used [14].

3.0.3 UV Diffuse Reflectance spectroscopy(UV DRS)

Is A sort of absorption spectroscopy known as diffuse reflectance spectroscopy measures the light that is reflected from the sample as opposed to the transmitted beam passing through it. This approach is frequently used to assess opaque materials that absorb too much energy to be detected through transmission. Diffuse reflectance spectroscopy is a technique used to collect and analyze scattered IR energy, which in turn is used to measure extremely fine particles or course surfaces[15]. UV–Vis Diffuse Reflectance Spectroscopy is a widely used, basic spectrophotometric technique for the analysis of powders and surfaces, requiring a negligible sample preparation . It is based on the surface dispersion of a fraction of the uv-Vis incident radiation on it[16].

Connect the UV visible spectrometer to the computer .Here, the solid sample was put in the sample holder and it was spread throughout the holder with the help of a pestle. This was then placed in the UV diffuse reflectance set up. There are four slots where in three slots contained barium sulphate powder and in the fourth slot, one has to place their sample.

3.0.4 Photoluminescence (PL)

PL is the Interaction between light and matter .Spectroscopy using photoluminescence operates in a non-contact mode. This method of analyzing the electrical structure of a substance is non-destructive. When light strikes a sample, a process known as photo-

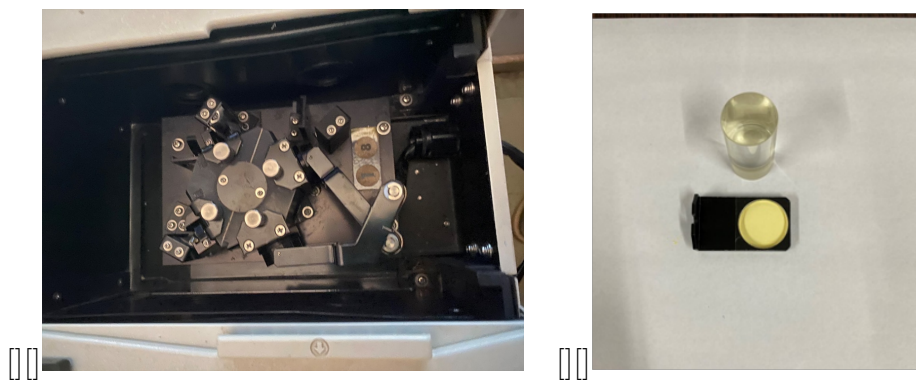


Figure 3.3: UV DRS Setup

excitation causes the light to be absorbed by giving the material its excess energy. Luminescence, or the emission of light, is one way that the sample dissipates this surplus energy. Luminescence in the context of photo-excitation is referred to as photoluminescence. Electrons in the material occupy the permitted excited states upon excitation. These excited electrons dissipate the excess energy as light, which is known as a radiative process, or as any other non-radiative process, returning to their stable, or equilibrium, or ground state. The energy difference between the two electronic states involved in the transition between the excited and equilibrium states is related to the light energy released (photoluminescence). On the other hand, the radiative process component determines how much light is released.[17]



Figure 3.4: Photoluminescence Setup

3.0.5 Flourescence

A small rectangular Box like setup wherein you have to place the liguid solutions inside the box. Three switches for three different type of wavelength are available. You can turn the switch on the switch of the desired wavelength and check if your liquid sample so prepared exhibited flourescences.

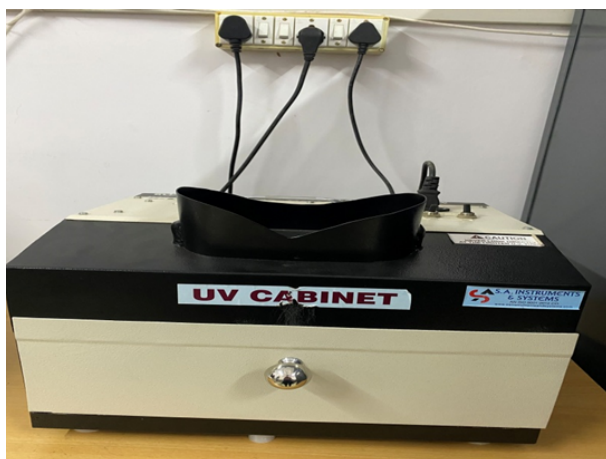


Figure 3.5: Flourescence Setup

Chapter 4

Results and Discussion

4.0.1 Characterisations

With a scan rate of $5^{\circ}/\text{min}$, an X-ray diffraction spectrometer (Cu K, $\lambda = 1.5415$) was used to examine the crystalline structures of g-C₃N₄. The amount of light that a material emits after absorbing photons was investigated using PL. Using absorbance spectroscopy, the catalysts' UV-vis absorbance in the 200–800 nm wavelength range was determined. Using UV diffuse reflectance spectroscopy, the band gap of g-C₃N₄, ZnO, and the g-C₃N₄/ZnO Composite were determined.

4.0.2 PXRD Analysis

PXRD was used to describe bulk g-C₃N₄ made by annealing melamine at 550°C (Figure 17). The strongest peak at $2\theta = 27.5^{\circ}$ is associated with the (002) g-C₃N₄ planes' interlayer stacking. The nitrogen-linked heptazine units' in-plane ordering is associated with the (100) planes, which are responsible for the peak at $2\theta = 12.8^{\circ}$ [18]. According to published g-C₃N₄ [19], the prominent peak at 27.5° in the g-C₃N₄ sample with an interplanar spacing of 0.323 nm corresponds to the multilayer stacking of conjugated aromatic systems. By using Scherrer's formula,

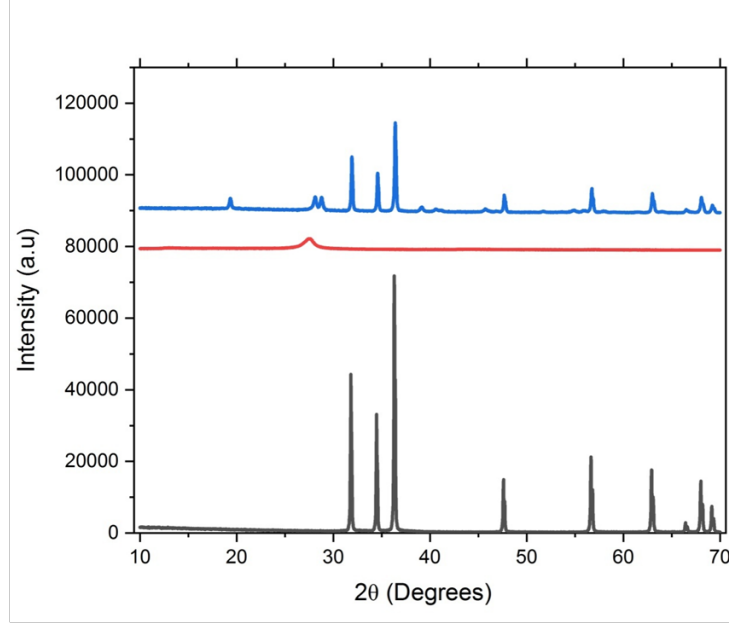


Figure 4.1: XRD graph for Bulk $g\text{-C}_3\text{N}_4/\text{ZnO}$, bulk $g\text{-C}_3\text{N}_4$ and bulk ZnO

$$D = \frac{(0.9\lambda)}{\beta \cos \delta}$$

, where β is the Full Width Half Maximum on the 2θ scale, θ is the Bragg's diffraction angle, and λ is the wavelength of the X-rays employed, which is Cu K radiation (1.5406 \AA). to calculate the FWHM of the sharpest diffraction peak corresponding to the (101) plane of the $g\text{-C}_3\text{N}_4 / \text{ZnO}$ nanocomposites, the crystallite sizes (D) of the ZnO nanoparticles in the $g\text{-C}_3\text{N}_4 / \text{ZnO}$ nanocomposites were found.[20]

4.0.3 Raman Spectroscopy

The Raman spectra of pristine $g\text{-C}_3\text{N}_4$, the unadulterated $g\text{-C}_3\text{N}_4$, the G mode around 1590 cm^{-1} emerging from sp^2 C particles and the D mode is showed up around 1340 cm^{-1} emerging from sp^3 C molecules, which may be ascribed to surface defects and disarranges[2].

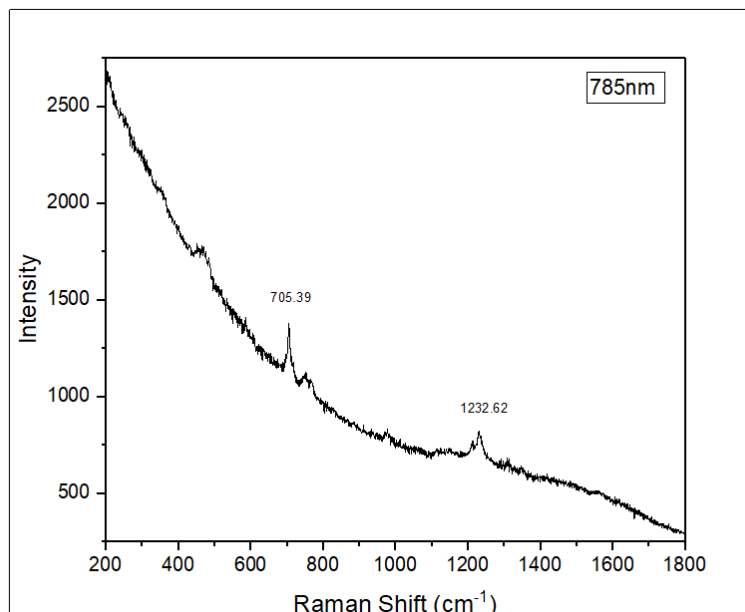


Figure 4.2: Raman Graph for g-C₃N₄

4.0.4 Optical Properties

The optical absorption characteristics of the produced samples were assessed using UV–vis absorption spectra. As shown in Fig. 17, the spectra were obtained in the 300–600 nm wavelength range. At 466 nm, the bare g-C₃N₄ sample exhibits a distinctive absorption peak whereas the bare ZnO sample exhibits a distinctive absorption peak at 390 nm. Additionally, we note that in the UV–Vis wavelength range, the absorbance of the g-C₃N₄/ZnO nanocomposite sample is marginally higher than that of the g-C₃N₄ sample that is the absorption peak for g-C₃N₄/ZnO is 478 nm. When compared to the naked g-C₃N₄ and ZnO samples, the absorption character of the g-C₃N₄/ZnO nanocomposites increases throughout the visible spectrum. This improved light absorption intensity in the visible range will be beneficial for the photocatalytic degradation process[18]. Compared to bare g-C₃N₄, the UV–vis absorption spectra of g-C₃N₄/ZnO nanocomposites show a progressive shift in absorption maxima. The evaluation of the bandgap energy levels for the produced materials was made possible by plotting Tauc’s graphs, as demonstrated using the provided typical Eq:

$$(\alpha h\nu)^2 = A(h\nu - E_g)$$

where $h\nu$ is the photon energy, A is the parameter, and α is the absorption coefficient. The indirect bandgap energy values for the g-C₃N₄ and g-C₃N₄/ZnO hybrid nanostructures were found using the Tauc plot between $(\alpha h\nu)^{1/2}$ as a function of $h\nu$ and extrapolating the straight-line portion to $(\alpha h\nu)^2$ the direct bandgap energy value for the ZnO nanoparticles was found using the Tauc plot between $(\alpha h\nu)^{1/2}$ a function of $h\nu$. ZnO and g-C₃N₄ are found to have bandgap energy values of 3.32 eV and 2.72 eV, respectively whereas the bandgap energy of the g-C₃N₄/ZnO hybrid nanostructures is 2.64 eV. The decrease of bandgap energy of g-C₃N₄/ZnO hybrid nanostructures can be ascribed to the effective interaction between g-C₃N₄ and ZnO, which has improved the photocatalytic degradation of dye under visible light irradiation[21].

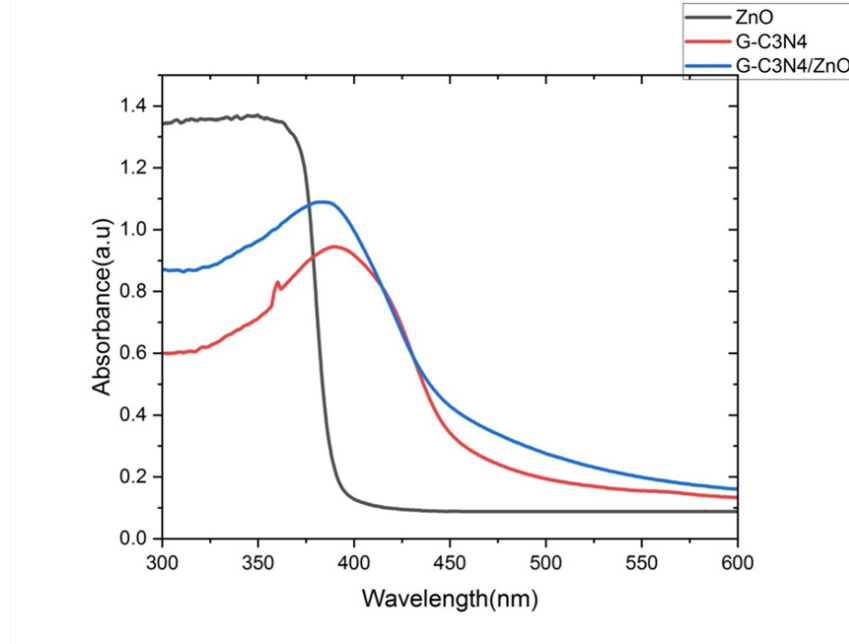


Figure 4.3: UV - DRS graph for Bulk g-C₃N₄, bulk ZnO and bulk g-C₃N₄/ZnO

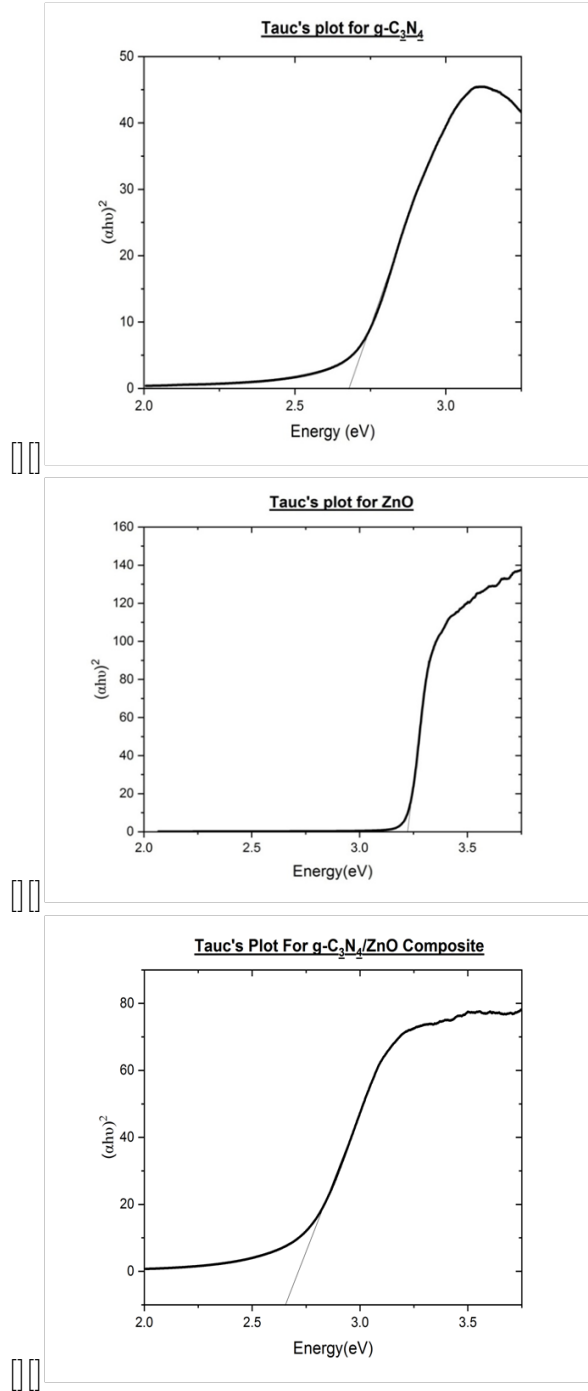


Figure 4.4: Tauc's plot for direct band gap for Bulk $g\text{-C}_3\text{N}_4$, bulk ZnO and $g\text{-C}_3\text{N}_4/\text{ZnO}$ composite respectively

SAMPLE	ABSORBANCE	BAND GAP (eV)
ZnO	390	3.23
Bulk $g\text{-C}_3\text{N}_4$	466	2.72
Calc $g\text{-C}_3\text{N}_4/\text{ZnO}$	478	2.64

Table 4.1: Displays the absorbance peak and the band gap for ZnO, $g\text{-C}_3\text{N}_4$ and the composite

4.0.5 PL Study

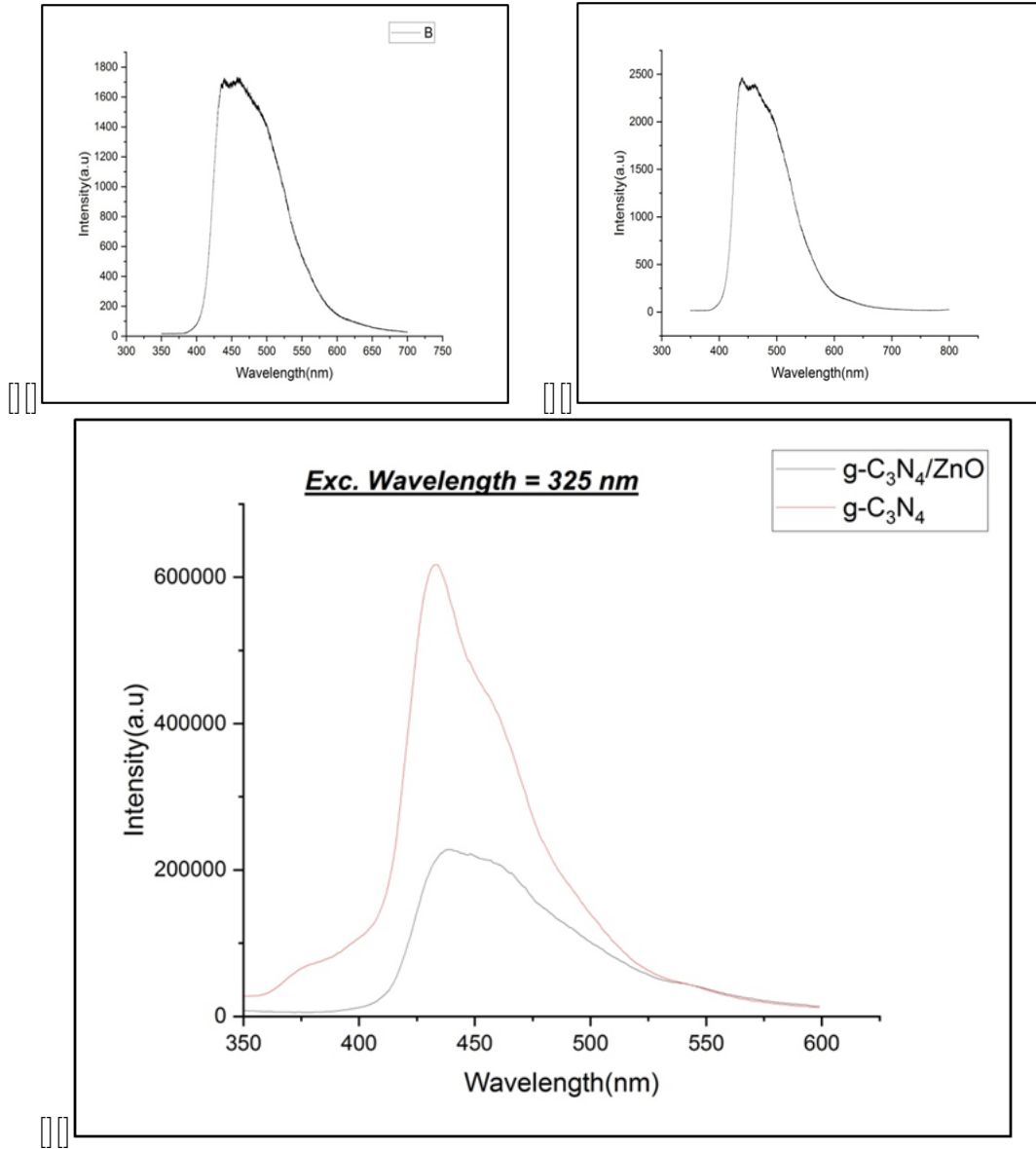


Figure 4.5: PL graph for (a) Bulk $\text{g-C}_3\text{N}_4$ (b) calc. $\text{g-C}_3\text{N}_4$ and (c) comparison of $\text{g-C}_3\text{N}_4$ and $\text{g-C}_3\text{N}_4/\text{ZnO}$

The PL spectrum absorption intensity of $\text{g-C}_3\text{N}_4/\text{ZnO}$ composite is significantly lower than those of pure $\text{g-C}_3\text{N}_4$ and pure ZnO , revealing a decrease in charge carrier recombination for composites[19]. The synthesized samples' separation and transfer efficiency of photoinduced charge carriers can be observed using the photoluminescence emission spectra that result from their recombination. Displays PL emission spectra measured at room temperature with an excitation wavelength of 325 nm. An intense broad emission peak is seen in the $\text{g-C}_3\text{N}_4$ sample at around 466 nm, which is the result of photoinduced

electron-hole pair radiative recombination.

The g-C₃N₄/ZnO nanocomposite samples, on the other hand, exhibit a sharp decline in intensity at this wavelength, suggesting that photoinduced electron-hole pair reunion is successfully blocked. The enlarged photoluminescence spectra of each sample within the wavelength range of 350–450 nm are shown in the g-C₃N₄ /ZnO graph. Large band gap ZnO (NBE) emission is the source of the emission peaks observed in the composites at 390 nm.

The photoluminescence mechanism is described here in order to comprehend the photoinduced charge separation and transfer in the produced photocatalysts. Electrons from the valence band go to the conduction band, leaving the holes in the former, when the g-C₃N₄ is activated by an excitation wavelength of 325 nm. After releasing their energy, the transferred electrons in the conduction band recombine with the holes in the valence band, producing PL emission.

The g-C₃N₄ sample's increased photoluminescence intensity is indicative of a higher rate of photoinduced electron-hole pair recombination. In the case of g-C₃N₄ /ZnO nanocomposites, the photoinduced electrons from the conduction band of g-C₃N₄ are transferred to the conduction band of ZnO, as the conduction band edge potential of g-C₃N₄ (-1.12 eV) is more negative than that of ZnO (-0.2 eV). The holes in ZnO's valence band moved to g-C₃N₄'s valence band in the interim. The recombination process in the g-C₃N₄/ZnO composite samples is successfully inhibited by the separation and transfer of charge carriers, which results in the observed decreased PL intensity.

The intensity of g-C₃N₄/ZnO nanocomposite is the minimal among all the composites indicating that the luminescence is quenched more effectively which in turn suggests the promoted photoinduced electron-hole pair separation and transfer[20].

4.0.6 Fluorescence

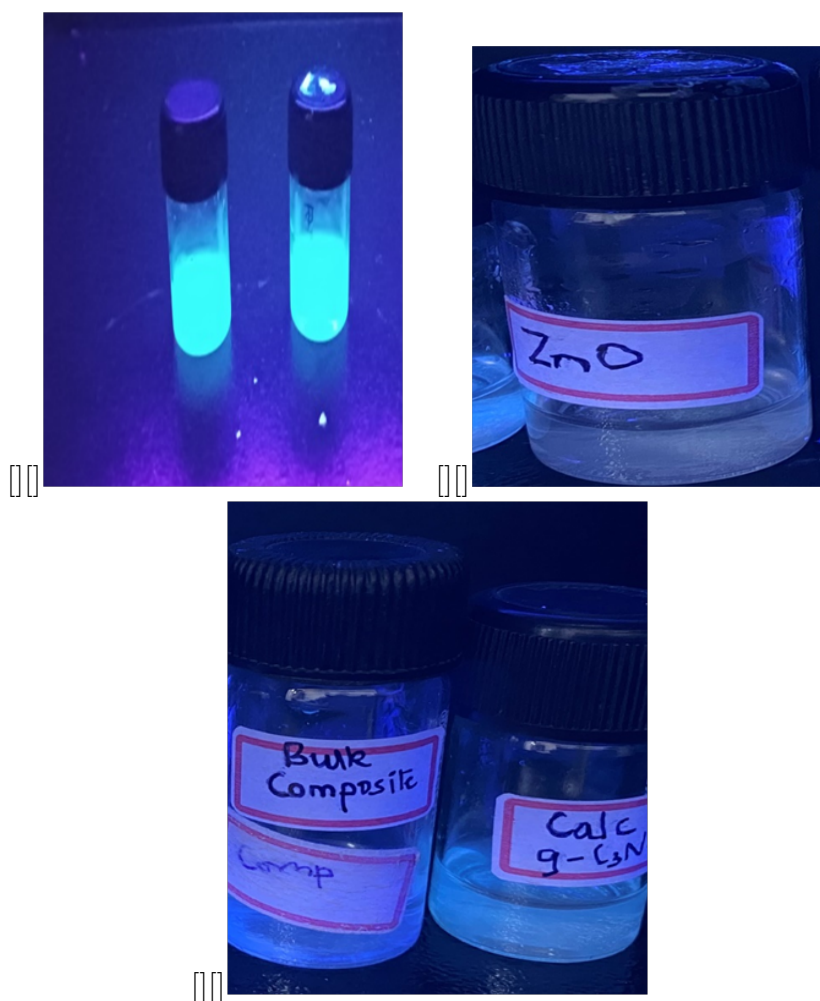


Figure 4.6: PL graph for (a) Bulk $\text{g-C}_3\text{N}_4$ (left) and Calc. $\text{g-C}_3\text{N}_4$ (right) b) Bulk ZnO and (c) bulk $\text{g-C}_3\text{N}_4/\text{ZnO}$ and Calc. bulk $\text{g-C}_3\text{N}_4/\text{ZnO}$

The phenomenon known as fluorescence occurs when a molecule absorbs electromagnetic radiation, usually from visible or ultraviolet light, and then releases a photon with a lower energy. A solution was prepared wherein 5 mg of the sample was dissolved in 5 ml of distilled water. The solvent used here was distilled water. These samples when placed under the fluorescence setup, it was observed that the calcinated $\text{g-C}_3\text{N}_4$ exhibited the most fluorescence then compared to the other samples.

4.0.7 Photocatalytic Performance

The generated bare ZnO, bulk g-C₃N₄, calcinated g-C₃N₄, and Bulk g-C₃N₄/ZnO and Calcinated g-C₃N₄/ZnO hybrid nano structures were tested for their ability to catalyze photo degradation of MB dye under exposure to visible light. Prior to assessing the produced samples photo catalytic potential, the MB dye's adsorption capacity was assessed. Before being exposed to visible light, the dye solutions containing photo catalyst were agitated for 60 minutes (that is 15 Minutes of ultra sonication and 45 minutes of magnetic stirring) in the dark to achieve the equilibrium between adsorption and desorption. The dye solution was then transferred into the photoreactor chamber and was exposed to light photons after 60 minutes. Under comparable reaction circumstances to those shown in the photocatalytic experiment, a control experiment for the photodegradation of MB dye without a photocatalyst was also carried out. All of the photocatalytic tests carried out in the presence of photocatalysts were typically conducted under starting dye concentration, and catalyst dose amounts.

The absorbance of the UV-vis absorption spectral peaks was taken into consideration while evaluating the Absorbance values of MB dye at different time intervals. here, throughout the experiment a interval of 10 mins was taken upto 120 minutes. Specifically, the MB dye's time-dependent UV-vis absorption spectra are shown, showing how well ZnO, bulk g-C₃N₄, bulk g-C₃N₄/ZnO (50 percent) photo catalysts perform in photodegradation.

As seen in Fig. 23, although apparent degradation of MB dye is reported under visible light exposure over the pure ZnO and g-C₃N₄ catalysts, the self-degradation of MB dye is very low under exposure to visible light in the absence of a catalyst, indicating that MB dye is significantly stable in the absence of a catalyst under visible light illumination [22].

It was seen as per the percent Degradation calculations, the MB dye could degrade only upto 13 percent on its own. Bulk ZnO showed a degradation of 44.49 percent and bulk g-c₃n₄ showed a degradation of 50.2 percent.

Conversely, when g-C₃N₄/ZnO hybrid nanostructures are present during photocatalysis tests, there is a significant decrease in the MB dye concentrations. Furthermore, combining ZnO nanoparticles with g-C₃N₄ changes the photocatalytic performance of g-C₃N₄ nanosheets significantly, and the greatest photodegradation efficiency of the g-C₃N₄/ZnO (50 percent) hybrid nanostructured photocatalyst is found.

The intensity of the spectral lines has shown a gradually decreasing pattern with increasing irradiation time, as shown in the time-dependent UV-vis absorption spectra of MB dye. After 120 minutes of light irradiation, the intensity kept decreasing[23]. It was discovered that practically all of the MB dye had photo-mineralized into a non-hazardous substance. Furthermore, it was shown that the ZnO nanoparticles effectively improved the photocatalytic activity of g-C₃N₄ nanosheets. Nevertheless, if the ZnO percentage in g-C₃N₄ is increased to more than 50 percent, the photodegradation efficiency is observed to be somewhat decreased[5].

When compared to bare g-C₃N₄ and ZnO photocatalysts, the enhanced ability to absorb visible light and the impediment in the electron-hole recombination rate could be the cause of the rise in photocatalytic performance of g-C₃N₄ with increasing ZnO content. The layered structure of g-C₃N₄ has facilitated the transfer of photogenerated electrons from g-C₃N₄ to ZnO due to the creation of heterojunction, and the presence of additional surface active sites on the g-C₃N₄ surface boosted the adsorption rate of dye molecules. As a result, it is established that the g-C₃N₄/ZnO(50 percent) hybrid nanostructured catalyst has an extraordinarily high photodegradation performance compared to both pure g-C₃N₄ and ZnO photocatalysts and other g-C₃N₄ZnO hybrid nanostructured photocatalysts.

Although a significant decrease in photodegradation activity is seen with increasing ZnO content in g-C₃N₄ nanosheets, this could be because of an increase in bandgap energy and a reduction in surface active sites brought on by a decrease in g-C₃N₄ content relative to ZnO in hybrid nanostructures. Simultaneously, in order to verify if the calcination had any effect on the photocatalytic degradation, the bulk samples were calcinated and these samples were also used for the study. As per the percentage degradation calculations, the

calcinated gg-C₃N₄ showed 50.2 percent whereas the calcinated g-C₃N₄/ ZnO Showed the highest degradation of 90.73 percent.

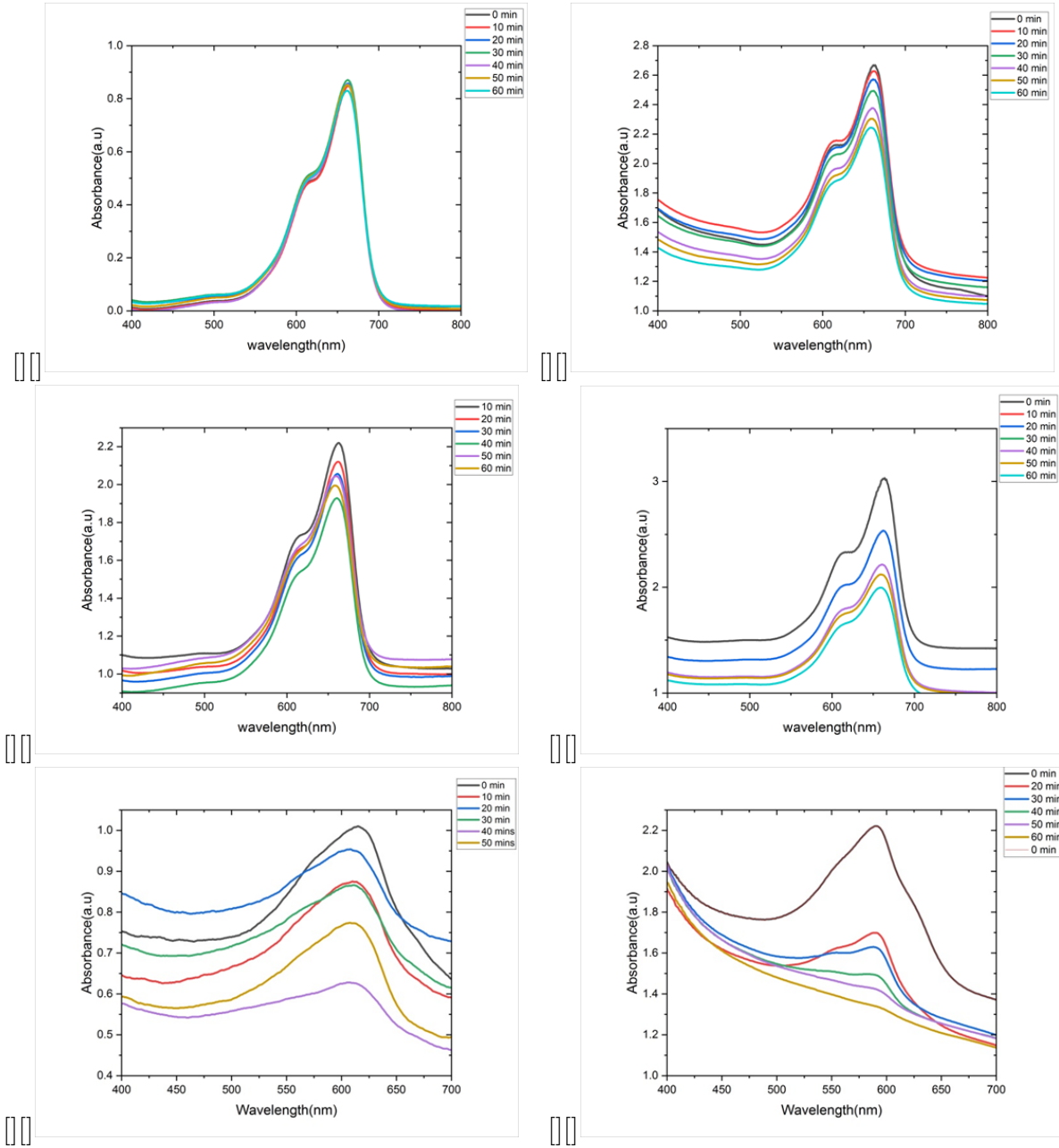


Figure 4.7: Photo degradation Graph for(a) MB Dye ,(b) Calc. ZnO , (c) Bulk g-C₃N₄,(d)calc. g-C₃N₄, (e) Bulk g-C₃N₄/ZnO , (f) Calc. g-C₃N₄/ZnO

SR NO.	PARAMETERS	% DEGRADATION
1.	Methylene Blue Dye	13.75
2.	10 mg-g-C ₃ N ₄ (Thiourea,Bulk)-5 ppm	14.39
3.	20 mg-g-C ₃ N ₄ (Thiourea,Bulk)-5 ppm	31.9
5.	100 mg-g-C ₃ N ₄ (Thiourea,Bulk)	31.80
6.	10 mg-g-C ₃ N ₄ (Thiourea,Calc)	32.24
7.	100 mg-g-C ₃ N ₄ (Melamine,Bulk)	39.00
8.	50 mg-g-C ₃ N ₄ (Thiourea, Calc)	50.4
9.	100 mg-g-C ₃ N ₄ (Melamine, Calc.)	52.38

Table 4.2: The various photocatalytic studies that are done by varying various parameters.

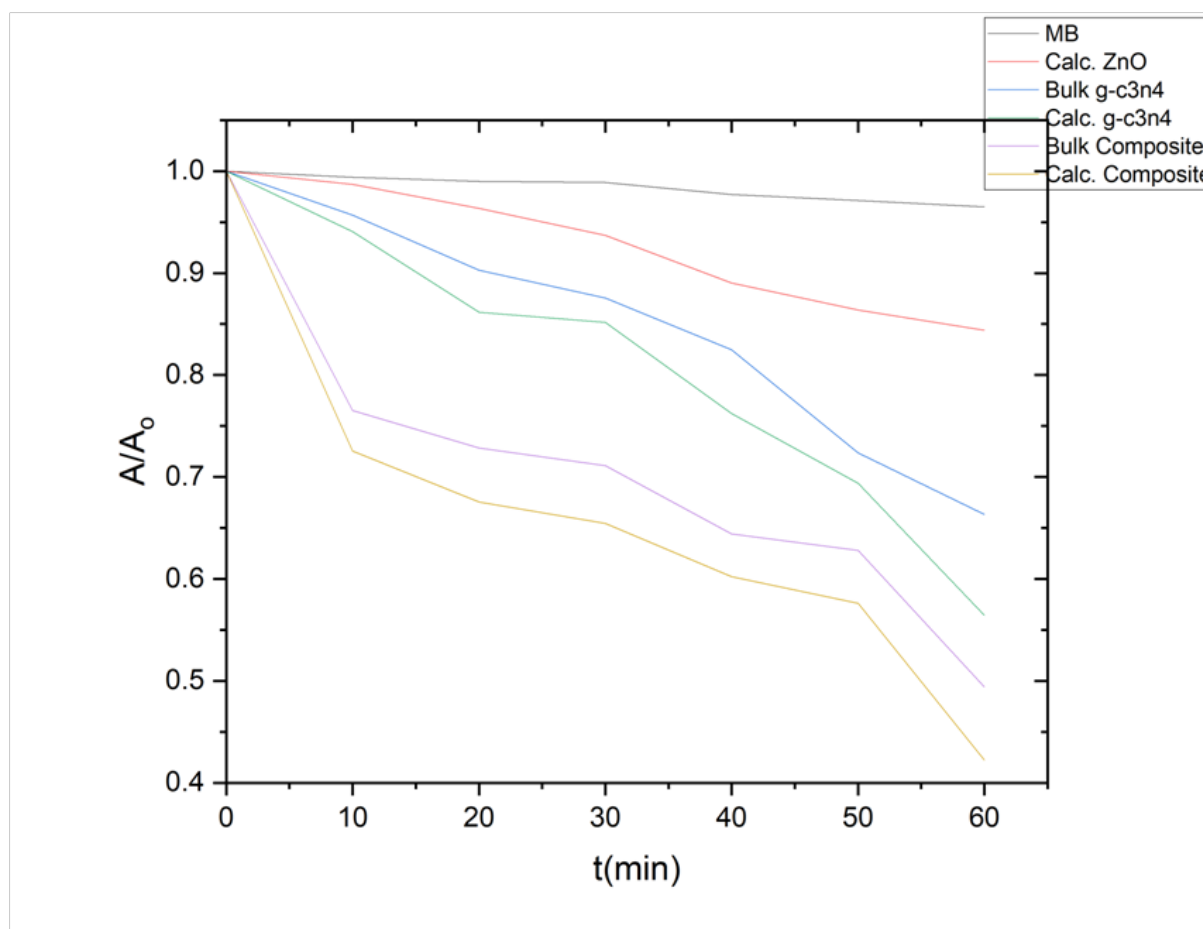


Figure 4.8: Graph of A/A_0 versus time (mins)

SAMPLE	RATE CONSTANT (min^{-1}) $\times 10^{-3}$	% DEGRADATION
MB	1.11	13.75
Calc. ZnO	6.43	32.24
Bulk g-C ₃ N ₄	11.05	50.42
Calc. g-C ₃ N ₄	11.30	52.38
Bulk g-C ₃ N ₄ /ZnO	37.23	88.56
Calc. g-C ₃ N ₄ /ZnO	39.66	92.05

Table 4.3: The Rate Constant and the % Degrdation to the corresponding Sample.

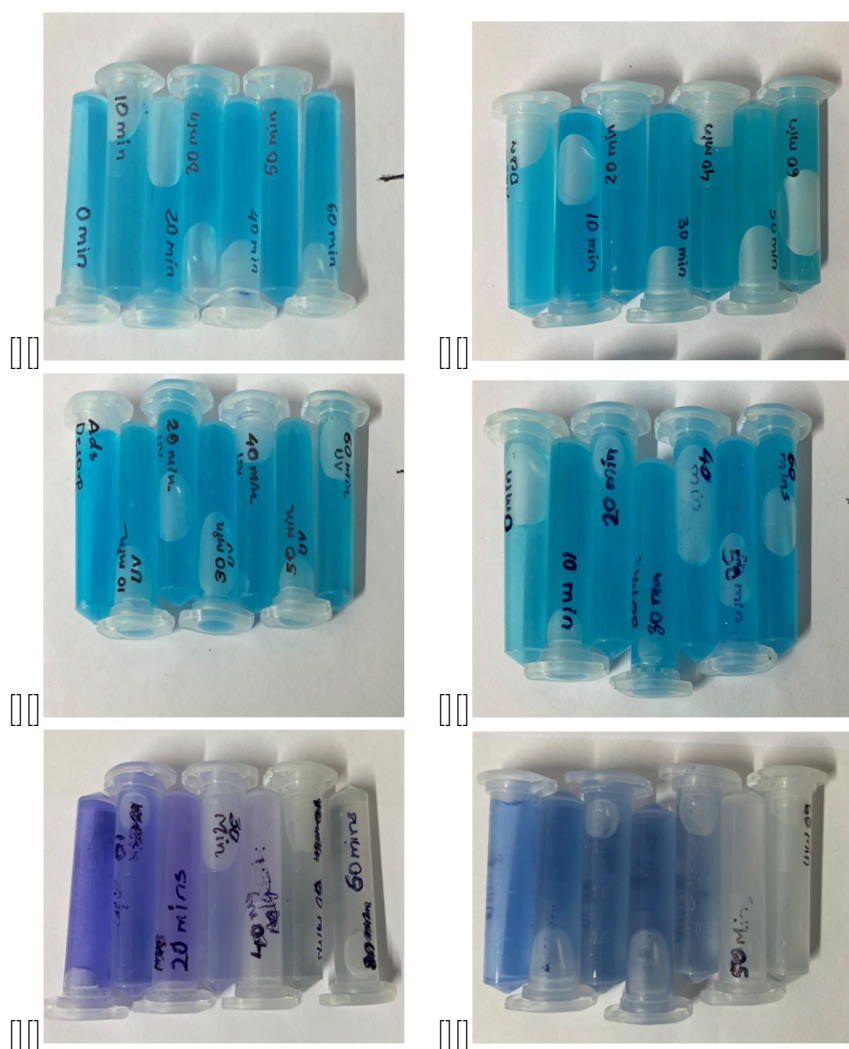


Figure 4.9: Colour degradation Graph for(a) MB Dye ,(b) Calc. ZnO , (c) Bulk g-C₃N₄,(d) calc. g-C₃N₄, (e) Bulk g-C₃N₄/ZnO , (f) Calc. g-C₃N₄/ZnO

4.1 Factors affecting photocatalytic Activity

4.1.1 Effect of initial dye concentration

The initial dye concentration is an important factor that plays a vital role in the photodegradation process. Thus, the photocatalytic performance of the prepared optimized g-C₃N₄/ ZnO(50 percent) hybrid nanostructured photocatalyst (100 mg catalyst in 10 ppm dye solution) was examined against the degradation of MB dye at various initial concentrations changing from 10 to 100 mg/L under the visible light irradiation for 120 min. the maximum degradation efficiency for MB is determined for the 100 mg/L of initial MB concentration which was taken as an optimized dye concentration for further degradation experiments. At a lower initial concentration of dye, the lower efficiency observed might be due to the less amount of dye adsorbed on the catalyst surface consequently, most of the surface active sites at the surface of the catalyst remain unoccupied, as a result the lower degradation efficiency determined. However, at a higher initial dye concentration, the decrease in the degradation efficiency may be due to the decreasing penetration of light photons or suppression of the path length of photons At lower initial dye concentration, the lower efficiency observed might be due to the less amount of dye absorbed on the photocatalyst surface. Most of the surface active sites at the surface of the photocatalyst remain unoccupied, as a result causing lower degradation. More amount of dye causes more intense colour and adversely affecting the dye removal efficiency decreasing penetration of light into the pollutant.

4.1.2 Effect of catalyst Dose Amount

To study the effect of catalyst dose amount on the photodegradation efficiency of MB dye under visible light exposure, the dose amounts of the optimized g-C₃N₄, ZnO and g-C₃N₄/ZnO (both bulk and calcinated) catalyst were changed from 10 to 100 mg in the 10 ppm MB dye solutions. As the dose amount of the catalyst was increased , the photodegradation efficiency for the MB dye is also found to be increasing At lower amount of catalyst ,there is a possibility that there are less number of active sites available. When

the amount of catalyst was increased more than the optimised it further decrease in the degradation was seen due to the scattering of light photons and also because of poor penetration.

4.1.3 Effect of Calcination on bulk sample

A common method for creating photocatalytic materials is calcination, which involves heating a substance to extremely high temperatures. Calcination can have a significant effect on the photocatalytic activity.

The material's crystallinity may be enhanced by calcination [6]. Better defined crystal structures result from increased crystallinity, and this can speed up the charge transfer procedures involved in photocatalysis.

By eliminating volatiles and impurities, calcination can improve a material's surface area. More surface area means that there are more active sites available for photocatalytic processes.

Calcination can modify the surface chemistry of the material, leading to the formation of active surface sites or oxygen vacancies, which can promote adsorption and activation of reactant molecules.

The material may undergo phase changes as a result of calcination, which may result in the emergence of more active phases or crystalline structures that are more appropriate for photocatalysis.

By eliminating organic impurities or leftover compounds from the material, calcination can lower the photocatalytic effectiveness of the material by preventing them from acting as recombination sites for photogenerated charge carriers.

4.2 Mechanism

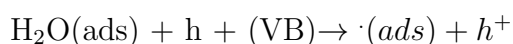
4.2.1 Mechanism of a photocatalyst

After absorbing light, a photocatalyst's mechanism involves creating electron pairs, which then produce hydroxyl and superoxide anion radical. These radicals subsequently react with various organic and inorganic pollutants and transform them into less or even non-toxic ions. Photocatalytic activity is triggered by a photoelectron being transported from the filled Valance Band to the empty Conduction Band by irradiation. The energy of a photon can either match or exceed the band gap of semiconductor photocatalysis. When the valence band of a semiconductor photocatalyst is irradiated with the conduction band, holes remain in the valence band. Electrons from the conduction band are absorbed by oxygen atoms absorbed by surface anions. This superoxide anion reacts with water to generate OH radicals that are responsible for decomposing pollutants.

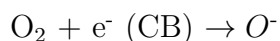
4.2.2 Mechanism of g-C₃N₄ as a photocatalyst



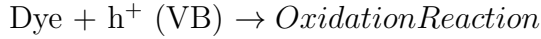
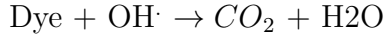
Photogenerated holes in the valence band react with water to generate \cdot radicals.



The OH \cdot Radical formed on the surface of the semiconductor are extremely powerful oxidizing agents. This radical attacks the adsorbed agent molecule or those that are very much close to the surface of the catalyst. While the photogenerated hole (h^+) reacts with the surface bound water or OH $^-$ to produce the hydroxyl radical, e^- in the CB is taken up by the oxygen in order to generate anionic superoxide radical.

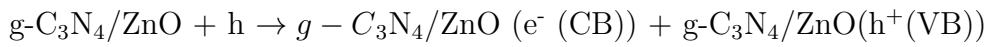


This superoxide ion doesnot only take part in the oxidation process but also prevent the e^-h^+ recombination thus maintaining electron neutrality.

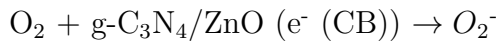


4.2.3 Mechanism of g-C₃N₄/ZnO as a photocatalyst

Upon irradiation of sun light , the e-h+ pairs at the g-C₃N₄/ZnO heterojunctions are generated and these pairs migrate to the surface.

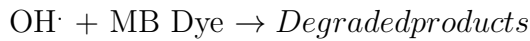
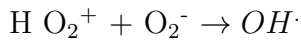


Then, at the CB of the g-C₃N₄/ZnO photocatalyst, the photo generated e⁻ reacts with the adsorbed O₂ on the surface to give superoxide radical.



The O₂⁻ subsequently reacts with MB dye to produce CO₂ and H₂O.

The O₂⁻ will then react with the H⁺ to produce the hydroxyl radical .The hydroxyl radical will react with the MB dye and give us the degraded products.



Due to the heterojunction photoexcited e⁻ and h⁺ are effectively getting separated .The surface charges will then react with the absorbed H₂O and O₂ on the photocatalyst surface to produce the highly unstable hydroxyl radical and superoxide radical which enhances the dye degradation efficiency[12].

References

- [1] Rui-Han Gao, Qingmei Ge, Nan Jiang, Hang Cong, Mao Liu, and Yun-Qian Zhang. Graphitic carbon nitride (g-c3n4)-based photocatalytic materials for hydrogen evolution. *Frontiers in Chemistry*, 10, Oct 2022.
- [2] Xiaojuan Bai, Li Wang, Ruilong Zong, and Yongfa Zhu. Photocatalytic activity enhanced via g-c3n4 nanoplates to nanorods. *The Journal of Physical Chemistry C*, 117(19):9952–9961, May 2013.
- [3] Radik R. Shamilov, Zufar M. Muzipov, Dmitriy O. Sagdeev, Kirill V. Kholin, Alina F. Saifina, Aidar T. Gubaidullin, and Yuriy G. Galyametdinov. Photocatalytic materials based on g-c3n4 obtained by the one-pot calcination method. *C*, 9(3):85, Sep 2023.
- [4] Zahra Mirzaeifard, Zahra Shariatinia, Milad Jourshabani, and Seyed Mahmood Rezaei Darvishi. Zno photocatalyst revisited: Effective photocatalytic degradation of emerging contaminants using s-doped zno nanoparticles under visible light radiation. *Industrial amp; Engineering Chemistry Research*, 59(36):15894–15911, Aug 2020.
- [5] Yue Sun, Wei Zhang, Qun Li, Huijie Liu, and Xiaolei Wang. Preparations and applications of zinc oxide based photocatalytic materials. *Advanced Sensor and Energy Materials*, 2(3):100069, Sep 2023.
- [6] Mahmudul Hassan Suhag, Aklima Khatun, Ikki Tateishi, Mai Furukawa, Hideyuki Katsumata, and Satoshi Kaneco. One-step fabrication of the zno/g-c3n4 compos-

- ite for visible light-responsive photocatalytic degradation of bisphenol e in aqueous solution. *ACS Omega*, 8(13):11824–11836, Mar 2023.
- [7] Ke Li, Miaomiao Chen, Lei Chen, Songying Zhao, Wencong Xue, Zixuan Han, and Yanchao Han. Synthesis of g-c3n4 derived from different precursors for photodegradation of sulfamethazine under visible light. *Processes*, 11(2):528, Feb 2023.
- [8] Ke Li, Miaomiao Chen, Lei Chen, Songying Zhao, Wencong Xue, Zixuan Han, and Yanchao Han. Synthesis of g-c3n4 derived from different precursors for photodegradation of sulfamethazine under visible light. *Processes*, 11(2):528, Feb 2023.
- [9] Xiwang Jiang, Jun Li, Jia Fang, Long Gao, Wenxuan Cai, Xiaoxia Li, Aihua Xu, and Xinchao Ruan. The photocatalytic performance of g-c3n4 from melamine hydrochloride for dyes degradation with peroxydisulfate. *Journal of Photochemistry and Photobiology A: Chemistry*, 336:54–62, Mar 2017.
- [10] Prami Nandi and Debajyoti Das. Synthesis of cost-effective g-c3n4/zno heterostructure photocatalyst for methyl orange (mo) dye degradation. *AIP Conference Proceedings*, 2020.
- [11] Jia-Xin Sun, Yu-Peng Yuan, Ling-Guang Qiu, Xia Jiang, An-Jian Xie, Yu-Hua Shen, and Jun-Fa Zhu. Fabrication of composite photocatalyst g-c3n4-zno and enhancement of photocatalytic activity under visible light. *Dalton Transactions*, 41(22):6756, 2012.
- [12] Abdullah M. Alhanash, Khadija S. Al-Namshah, Sahar K. Mohamed, and Mohamed S. Hamdy. One-pot synthesis of the visible light sensitive c-doped zno@g-c3n4 for high photocatalytic activity through z-scheme mechanism. *Optik*, 186:34–40, Jun 2019.
- [13] Libretexts. X-ray diffraction (xrd) basics and application, Aug 2022.
- [14] Mettler-Toledo International Inc. all rights reserved. Raman spectroscopy, May 2023.

- [15] Diffuse reflectance spectroscopy - an overview — sciencedirect topics.
- [16] Ultraviolet–visible diffuse reflectance spectroscopy (uv–vis drs), a rapid and non-destructive analytical tool for the identification of saharan dust events in particulate matter filters, Feb 2021.
- [17] Timothy H. Gfroerer. Photoluminescence in analysis of surfaces and interfaces. *Encyclopedia of Analytical Chemistry*, Oct 2000.
- [18] Buse Sert, Zeynep Bilici, Kasim Ocakoglu, Nadir Dizge, Tannaz Sadeghi Rad, and Alireza Khataee. Preparation of s-scheme g-c3n4/zno heterojunction composite for highly efficient photocatalytic destruction of refractory organic pollutant. *Catalysts*, 13(3):485, Feb 2023.
- [19] Xiuling Guo, Jihai Duan, Chaojie Li, Zisheng Zhang, and Weiwen Wang. Highly efficient z-scheme g-c3n4/zno photocatalysts constructed by co-melting-recrystallizing mixed precursors for wastewater treatment. *Journal of Materials Science*, 55(5):2018–2031, Oct 2019.
- [20] N Chidhambaram and K Ravichandran. Fabrication of zno/g-c3n4 nanocomposites for enhanced visible light driven photocatalytic activity. *Materials Research Express*, 4(7):075037, Jul 2017.
- [21] Parmeshwar Lal Meena, Krishna Poswal, Ajay Kumar Surela, and Jitendra Kumar Saini. Synthesis of graphitic carbon nitride/zinc oxide (g-c3n4/zno) hybrid nanostructures and investigation of the effect of zno on the photodegradation activity of g-c3n4 against the brilliant cresyl blue (bcb) dye under visible light irradiation. *Advanced Composites and Hybrid Materials*, 6(1), Dec 2022.
- [22] Buse Sert, Zeynep Bilici, Kasim Ocakoglu, Nadir Dizge, Tannaz Sadeghi Rad, and Alireza Khataee. Preparation of s-scheme g-c3n4/zno heterojunction composite for highly efficient photocatalytic destruction of refractory organic pollutant. *Catalysts*, 13(3):485, Feb 2023.

- [23] Renuka Garg, Renu Gupta, and Ajay Bansal. Synthesis of g-c3n4/zno nanocomposite for photocatalytic degradation of a refractory organic endocrine disrupter. *Materials Today: Proceedings*, 44:855–859, 2021.